Applied Catalysis B: Environmental 178 (2015) 91–99

Contents lists available at ScienceDirect

Applied Catalysis B: Environmental

journal homepage: www.elsevier.com/locate/apcatb

Direct growth of shape controlled TiO_2 nanocrystals onto SWCNTs for highly active photocatalytic materials in the visible

Francesca Petronella[a], M. Lucia Curri[a], Marinella Striccoli[a], Elisabetta Fanizza[b], Cintia Mateo-Mateo[c], Ramon A. Alvarez-Puebla[d,e], Teresa Sibillano[f], Cinzia Giannini[f], Miguel A. Correa-Duarte[c,*], Roberto Comparelli[a,*]

[a] CNR-IPCF, Istituto per i Processi Chimici e Fisici, U.O.S. Bari, c/o Dip. Chimica Via Orabona 4, 70126 Bari, Italy
[b] Università degli Studi di Bari–Dip. Di Chimica, Via Orabona 4, 70126 Bari, Italy
[c] Dpto. Química Física - Centro de Investigación Biomédica (CINBIO), and Instituto de Investigación Biomédica de Vigo (IBIV), Universidade de Vigo, 36310 Vigo, Spain
[d] ICREA, Passeig Lluís Companys 23, 08010 Barcelona, Spain
[e] Universitat Rovira i Virgili & Centro de Tecnologia Quimica de Cataluña, Carrer de Marcel•lí Domingo s/n, 43007 Tarragona, Spain
[f] CNR-IC–Istituto di Cristallografia, via Amendola 122/O, 70126 Bari, Italy

ARTICLE INFO

Article history:
Received 3 July 2014
Received in revised form 7 October 2014
Accepted 10 October 2014
Available online 22 October 2014

Keywords:
Carbon nanotube
Titanium dioxide
Visible light photocatalysis
Heterostructures
Shape control

ABSTRACT

We report a very effective synthetic approach to achieve the *in situ* growth, directly at the surface of single walled carbon nanotubes, of shape controlled anatase TiO_2 nanocrystals, either as nanorods or nanospheres, by simply tuning the ratio between reactants. Remarkably, the obtained SWCNTs/TiO_2 heterostructures result dispersible in organic solvents, leading to optically clear dispersions. The photocatalytic activity of the SWCNTs/TiO_2 heterostructures, compared with bare TiO_2 nanorods or nanospheres demonstrates a significant enhancement. In particular, SWCNTs/TiO_2 heterostructures demonstrates an enhancement of reaction rate up to 3 times with respect to the commercially available standard TiO_2 powder (TiO_2 P25) under UV light and up to 2 times under visible light.

1. Introduction

Photoactive nanomaterials have got paramount relevance during the last 20 years due to their ability to generate electron–hole pairs, under appropriate irradiation. Such a property can be exploited for potential application in photocatalysis, environmental remediation, self-cleaning of surfaces, new generation solar cells, hydrogen production, sensing [1–6]. One of the most promising photoactive nanomaterials is TiO_2 because of its high quantum yield, chemical stability, commercial availability and low cost. The two most photoactive crystalline phases of TiO_2 are anatase and rutile, being the former generally regarded as the most suitable for photocatalytic applications [7]. Nonetheless, the large scale application of TiO_2 nanomaterials is still prevented due to several problems related to their photocatalytic efficiency, their low absorption in the visible range and the technological issue of their immobilization and/or recovery for photocatalytic application [8].

The photocatalytic efficiency is linked to competition between life-time of photogenerated species and of their recombination which could occur either in the bulk of the material and/or at the surface sites. In addition, the presence of defects in TiO_2 lattice could promote charge carriers trapping thus preventing the interfacial charge transfer which is the *conditio sine qua non* to exploit photogenerated charges [9]. The photocatalytic efficiency of TiO_2 is affected not only by surface atomic structure, but also by size, shape, crystallinity, degree of exposure, and hence availability, of reactive crystal facets [10,11]. Indeed, the average surface energy of anatase TiO_2 facets is 0.90 J m^{-2} for{0 0 1}, 0.53 J m^{-2} for {1 0 0}, 0.44 J m^{-2} for {1 0 1} [10,12] and considering that highly reactive facets are expected to effectively enhance surface properties, enormous effort has been devoted to the preparation of (0 0 1) facet-dominated single-crystal anatase TiO_2 and to its application to photocatalysis [11]. Moreover only 4% of solar light can be effective in generating electron–hole pairs in TiO_2 [13] due to its wide band gap which strongly affects the efficiency of solar light activated processes.

* Corresponding authors.
E-mail addresses: macorrea@uvigo.es (M.A. Correa-Duarte), r.comparelli@ba.ipcf.cnr.it (R. Comparelli).

http://dx.doi.org/10.1016/j.apcatb.2014.10.030
0926-3373/

Therefore, the main current open questions for such a class of photoactive materials are: (i) reducing electron–hole pair recombination, (ii) increasing visible light absorption and (iii) controlling size, shape and crystalline phase of TiO_2 in order to enhance the surface-to-volume ratio and suitably tailor TiO_2 (photo)catalytic properties. Indeed, the ability in tuning size and shape can turn in the capacity of tailoring e^-/h^+ redox potential and exposed crystalline plane [14].

Several strategies have been proposed to cope with the first two issues including surface modification of the semiconductor particles with red-ox couples or noble metals and/or doping or coupling with narrower band gap semiconductors [13,15,16]. Particularly interesting is the recent work by Bian and co-workers, where they synthesized TiO_2 mesocrystals modified with plasmonic Au nanoparticles with improved photocatalytic activity in the visible for organic pollutant degradation. They showed an evident enhancement in photocatalytic performances of one order of magnitude higher than that found for common Au/TiO_2 nanoparticle systems. Such an excellent behaviour can be explained in terms of an effective slowdown of the charge recombination process of electrons and holes in the Au nanoparticles [17]. An emerging alternative relies on the coupling of TiO_2 nanocrystals with carbon nanotubes (CNTs) either multi- or single-walled [7,18]. Indeed, CNTs can potentially contribute to increase photocatalytic activity by acting on three distinct features: (i) providing high-surface area and, hence a high density of active sites for adsorption and catalysis, (ii) retarding electron–hole recombination and (iii) inducing visible light catalysis by modification of band-gap and/or sensitization [19]. Several studies on the development of CNT–TiO_2 hybrids for enhancing photocatalytic activity have been reported over the past decade [19–21]; however, a strong effort is still needed to design and control size, shape and crystalline phase of TiO_2 synthesized in presence of CNTs. It has been reported that a close contact between titania and CNTs is required in order to fully promote their interaction, and thus effectively exploit their synergic behaviour [22,23]. So far, only a few reports have accounted an effective control of TiO_2 morphological features in presence of CNTs, e.g. shell thickness of TiO_2 or nanocrystal shape of the titania grown on CNTs [21,24]. Indeed, up to now the most effective approaches for the control over the nanocrystal size and shape have been demonstrated based on binding of pre-synthesized nanoparticles onto the nanotube walls. Therefore, several steps are then generally required for fabricating CNT/inorganic-nanoparticle hybrids, and especially when use of anisotropic nanoparticles is planned [25,26].

In this work we report on a very effective colloidal synthesis to obtain just in one step *in situ* growth of anatase TiO_2 at the surface of single walled carbon nanotubes (SWCNTs), controlling the shape of TiO_2 as TiO_2 nanorods (NRs) or, alternatively, nanospheres (dots by simply tuning the ratio between reactants. Interestingly, the obtained SWCNTs/TiO_2 heterostructures resulted dispersible in apolar organic solvents as chloroform, hexane and toluene. They have been characterized by TEM, SEM, and Raman spectroscopy and their photocatalytic properties have been tested in the photocatalytic discolouration of a water soluble model compound (the azo-dye methyl red; MR) under UV and visible irradiation and compared with bare TiO_2 NRs, dots and with a commercially available standard TiO_2 powder (TiO_2 P25). Experimental results demonstrated that (i) the proposed synthetic procedure allows to obtain a high control over TiO_2 size and shape in the heterostructures; (ii) and that SWCNTs/TiO_2 hybrids show a significant enhancement of photocatalytic properties in the UV and visible range. In particular, SWCNT/TiO_2 shows a three-fold enhancement of kinetic constant with respect to standard commercially available TiO_2 under UV excitation and a two-fold enhancement under visible light irradiation.

2. Experimental

2.1. Materials

All chemicals were of the highest purity available and were used as received without further purification. (Titanium tetraisopropoxide (TTIP, 99.999%), trimethylamino-N-oxide anhydrous and dihydrate (TMAO, 98%), anhydrous ethylene glycol (EG, 98%) and oleic acid (OLEA, 90%) were purchased from Sigma-Aldrich. All solvents used were of analytical grade and purchased from Aldrich. Commercial TiO_2 is TiO_2 "Degussa P25" (TiO_2 P25), and Methyl Red (MR) is 2-(4-dimethylamino-pheny-lazo)-benzoic acid, C. I. 13020, MeRed, Sigma-Aldrich. SWCNTs (90% purity and low functionality) were purchased from Carbon Nanosolutions Inc. The process used by the company (air oxidation) for the purification ensure that the purified material closely aproximates to the pristine state with low functionality.

2.2. Synthesis of SWCNTs/TiO_2 heterostructures

SWCNTs were washed in an acetone/ethanol solution, sonicating under mild conditions (1 h). Afterwards the CNTs were dispersed in water by means of sonication (30 min). The resulting suspension was then frozen with liquid nitrogen, and dried CNTs were finally obtained through a lyophilization process. Then, the stock solution of SWCNTs in OLEA was prepared adding 0.1 mg of SWNTs to 20 mL of OLEA. The solution was then sonicated during 2 h and stored at room temperature in the dark. This stock solution was typically sonicated for 15 min just before using.

Two different methods were exploited to growth nearly spherical or rod-like TiO_2 nanocrystals, respectively.

2.3. Synthesis of SWCNTs/TiO_2 dots—Slow Hydrolysis Route

A defined amount of SWCNT stock solution in OLEA ranging from 0.47 g to 0.96 g was added to 35 g of OLEA in order to keep the TTIP:SWCNTs ratio in the range from 1500:1 to 6200:1. The mixture was sonicated for 15 min to allow SWCNT dispersion in OLEA. After that, 885 mg of anhydrous TMAO were added. The obtained mixture was degased for 15 min at 100 °C. Under nitrogen flux 2.3 mmol of TTIP were injected into the reaction flask. The solution turned from colourless to pale yellow, indicating the formation of a complex between OLEA and TTIP. 50–100 mmol of EG were subsequently added. The solution was kept in a close system and stirred at 100 °C over 5 days. Hydrolysis of the titanium dioxide precursor is thought to occur upon reaction with water released slowly upon esterification of OLEA and EG. The reaction was stopped by removing heating and a grey powder was recovered by adding ethanol or methanol. The SWCNTs/TiO_2 dots heterostructure was easily redispersed in apolar organic solvents as $CHCl_3$ or hexane.

2.4. Synthesis of SWCNTs/TiO_2 nanorods—Fast Hydrolysis Route

Rod-like nanoparticles were obtained. 1.8–5.4 g of SWCNTs OLEA stock solution were added to 35 g of OLEA in order to keep the TTIP:SWCNTs ratio in the range from 1000:1 to 3000:1 and the mixture sonicated for 15 min. The reaction mixture was then kept under vacuum at 100 °C for 15 min under vigorous stirring. Under nitrogen flow, 8 mmol of TTIP was added and the solution turned from colourless to pale yellow. At this stage, 2.5 mL of a 1 M aqueous base solution (TMAO dihydrate) was rapidly injected into the reaction mixture. The solution was kept in a closed system at 100 °C and stirred under mild reflux with water over 5 days to promote further hydrolysis and crystallization of the product. The reaction was stopped by removing heating and a grey powder recovered by

adding ethanol or methanol. The SWCNTs/TiO_2 NRs heterostructure was then dispersed in apolar organic solvents as $CHCl_3$, or hexane.

2.5. Synthesis of TiO_2 nanorods or dots

The synthesis of TiO_2 NRs or dots was performed according to the above reported procedures in absence of SWCNTs [27].

2.6. Transmission electron microscopy characterization

High resolution transmission electron microscopy (HRTEM) analysis was performed by a JEOL JEM-2010 FEG microscope operating at 200 kV. The HRTEM samples were prepared by casting a drop of SWCNTs/TiO_2.$CHCl_3$ solution onto a carbon hollowed TEM grid.

2.7. Scanning electron microscopy characterization

Field emission scanning electron microscopy (FE-SEM) was performed by a Zeiss Sigma microscope operating in the range 0.5–20 kV and equipped with an in-lens secondary electron detector. FE-SEM samples were prepared by casting a few drop of SWCNTs/TiO_2 $CHCl_3$ solution onto a silicon slide. Samples were mounted onto stainless-steel sample holders by using double-sided carbon tape and grounded by silver paste.

2.8. X-ray diffraction experiments and simulations

X-ray diffraction data were collected at room temperature from nanoparticles samples of both TiO_2 and SWCNTs/TiO_2 dots and nanorods deposited onto silicon substrates. Measurements were performed in coupled sample/detector ($\theta/2\theta$) scan mode (symmetric reflection geometry) by a Bruker D8 Discover diffractometer, equipped with a Göbel mirror, using Cu K_α radiation ($\lambda_{K\alpha1}$ = 1.54056 Å and $\lambda_{K\alpha2}$ = 1.54439 Å), and a scintillation detector. The working conditions were 40 kV and 40 mA. Data were collected in the range 10–100° with a step size of 0.05°.

2.9. FT-IR-ATR spectroscopic characterization

Mid-infrared spectra were acquired with a Varian 670-IR spectrometer equipped with a DTGS (deuterated tryglicine sulfate) detector. The spectral resolution used for all experiments was 4 cm^{-1}. For Attenuated Total Reflection (ATR) measurements the internal reflection element (IRE) used was a one bounce 2 mm diameter diamond microprism. Cast films have been prepared directly onto the internal reflection element, by depositing the solution or suspension of interest (3–5 μL) on the upper face of the diamond crystal and allowing the solvent to evaporate.

2.10. Raman spectroscopic characterization

Raman experiments were conducted in a micro-Renishaw InVia Reflex system. The spectrograph uses a high resolution grating (1800 grooves cm^{-1}) with additional band-pass filter optics, a confocal microscope and a 2D-CCD camera. Excitation was carried out at using a laser line at 633 nm with acquisition times of 10 s. Laser was focused on the sample by using a ×50 objective with power at the sample of 10 mW. For the conversion with the irradiation time, the same parameters were used. For semi-quantitative analysis, bands were deconvoluted by Lorentzian shape, where the band position and the full widths at half maxima were fixed after applying a linear baseline (Fig. 3c) [28].

2.11. Photocatalysis experiments

In a typical experiment, 0.01 mmol of TiO_2-based catalysts was deposited onto a glass slide (with a surface of 3.6 cm^2) by dropping the proper amount of catalyst solution and letting the solvent to evaporate, thus leading to nearly transparent films. The concentration of the catalyst solution has been calculated by atomic absorption spectroscopy. Control experiments were carried out in presence of the same amount of SWCNTs exploited in the synthesis of the SWCNTs/TiO_2 catalyst. Briefly, the proper amount of the SWCNT stock solution was washed three times with ethanol in order to remove the excess of OLEA, redispersed in chloroform and cast onto the glass slide. Further control experiments were carried out in presence of mixtures consisting in pre-synthesized TiO_2 nanocrystals (dots or rods) and SWCNTs with the same mass ratio exploited in the synthesis procedure and comparable amount of TiO_2 Finally control experiments at the dark were performed in order to evaluate the role played by adsorption in dye discolouration.

The transparent glass support was suitably shaped in order to fit a 1 cm × 1 cm quartz cell and positioned against the cuvette wall, further with respect to the light beam. A medium-pressure 200 W mercury lamp (λ > 250 nm) was used as radiating source for experiments with UV light. Photocatalytic experiments under visible light were performed by a 250 W quartz tungsten halogen lamp, filtered by band pass filter to transmit light from 430 nm to 3300 nm [29]. All experiments were performed under ambient atmosphere, keeping the system under vigorous stirring. At a fixed illumination time, samples of the solution were withdrawn from the reaction batch in order to monitor the discolouration course by UV–Vis absorption spectroscopy. The pH value was adjusted by adding the proper amount of 0.1 M HCl. A possible leaching of TiO_2 in the aqueous solution during photocatalysis was investigated by ICP analyses on water treated with our catalysts and Ti amount was found below the detection limit.

3. Results and discussion

3.1. Synthesis of SWCNTs/TiO_2 heterostructures

The proposed synthetic procedure is based on a careful adjustment of reported synthetic protocols for the one-pot synthesis of rod-like or spherical anatase TiO_2 nanocrystals [27]. The synthesis is promoted by the hydrolysis of titanium isopropoxide (TTIP) catalysed by trimethylamino-N-oxide dehydrate (TMAO) in the presence of oleic acid (OLEA) as capping agent and carried out at relatively low temperature (100 °C) under standard air-free conditions. Here the synthetic conditions have been adapted to promote the nucleation of TiO_2 NRs or dots at the surface of SWCNTs. Indeed, the presence of an excess of water has been reported to promote anisotropic growth leading to nanorods (*fast hydrolysis route*), whereas when the presence of a stoichiometric amount of water, generated through an esterification reaction occurring between OLEA and glycerol, leads to isotropic growth, resulting in nearly spherical nanocrystals (*slow hydrolysis route*).

Defined ranges of Ti/SWCNT ratios, namely from 1000:1 to 3000:1 for rods and from 1500:1 to 6200:1 for dots, have been investigated for the synthesis of NRs and dots TiO_2 nanocrystals, respectively. However, the morphological and structural features of SWCNTs/TiO_2 heterostructures have been found to not be affected by the Ti/SWCNT. The reaction has been carried out for 5 days to promote anatase phase nucleation and to allow TiO_2 surface reconstruction [27]. The reaction product has been recovered by adding a non-solvent (ethanol or methanol) with subsequent centrifugation. Remarkably the obtained gray powder has been found dispersible

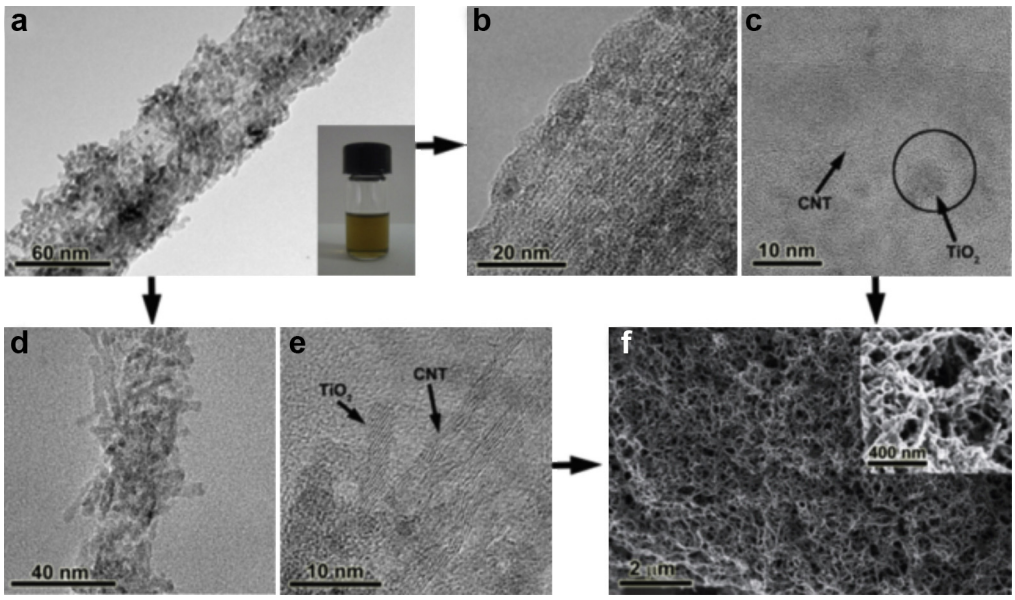

Fig. 1. Transmission (A–E) and scanning (F) electron microscopy images of a typical SWCNTs/TiO_2 sample. High resolution-TEM images of SWCNTs coated with TiO_2 dots (B, C) and SWCNTs coated with TiO_2 NRs (A, D, E). The inset in (F) shows a higher magnification SEM image of SWCNTs/TiO_2 NRs.

in nonpolar solvents (chloroform, hexane, and toluene) leading to optically clear dispersions and thus providing a preliminary experimental evidence that SWCNT surface modification took place (see inset in Fig. 1a and Figure S1 in Supplementary Material). OLEA has been selected as a suitable medium to disperse SWCNTs in order to promote the dispersion of SWCNTs in the reaction flask, being OLEA the coordinating solvent of TiO_2 nanocrystals. It is worth to observe that bare SWCNTs, employed in the present work, are not functionalized by chemical treatments as strong acid oxidation in order to preserve their optoelectronics properties [30] and have been found not dispersible at all neither in organic solvent nor in water. Separation of bare TiO_2 nanocrystals possibly nucleated far-off the SWCNTs/TiO_2 heterostructures has been performed by centrifuging at 2500 rpm for 5 min, the obtained organic dispersion without adding any precipitating agent. Indeed, upon centrifugation, due to their low weight, bare TiO_2 nanocrystals have been found stable in the solvent, without precipitating. On the other hand a grey powder, much heavier, has been collected at the bottom of the tube. Such a grey powder, redispersed in organic solvents after the centrifugation cycle, has finally resulted formed of SWCNTs/TiO_2 heterostructures, as clearly pointed out by TEM.

3.2. Structural and optical characterization

The samples of SWCNTs/TiO_2 heterostructures for structural, optical, and photocatalytic characterization have been washed several times (from 5- to 10 times) to remove any excess of OLEA, either free and coordinated at the surface of TiO_2 by adding ethanol or methanol to the organic solution and collecting the precipitate by centrifugation.

Transmission and scanning electron microscopy images (Fig. 1) show TiO_2 NRs (19×3 nm; standard deviation 6%; Fig. 1a, d, e, S2) or dots (diameter 6 ± 0.5 nm; Fig. 1b and c) grown on SWCNT surface. TiO_2 NRs have been found to randomly grow onto the SWCNT surface both horizontally, i.e. along the long side of the rod in contact with SWCNTs, (Figure S2 Supplementary Material) or vertically with respect to SWCNT surface, i.e. with NRs tip in contact with SWCNTs.

High magnification micrographs (Fig. 1c and e) point out the crystalline domain of TiO_2 dots or NRs in contact with the crystalline planes of SWCNTs. The obtained TiO_2 NRs exhibit an anatase crystalline structure as indicated in Fig. 2 and S2 [27].

They have a longitudinal axis (*c*-axis) in the ⟨0 0 1⟩ direction that is parallel to the {0 1 0} type facets; being the latter the most developed facets of the NRs (see Figure S2). Typically the {0 1 0} facet should have a larger surface interacting with the surface of the CNTs. However some rods have been found to show the {0 0 1} facet, hence the tip, binding the CNTs surface. Fig. 1f and its inset show SEM micrographs of a typical bundle in which SWCNT surface is completely covered by TiO_2 dots. SEM images clearly demonstrate the close packed arrangement of TiO_2 nanocrystals around SWCNTs.

To further confirm the actual growth of the TiO_2 nanostructures detected in the TEM/SEM images actually on the surface of SWCNTs, pre-synthetized TiO_2 NRs have been mixed with SWCNTs. The SEM micrograph of the mixture (Figure S3 in Supplementary Material)

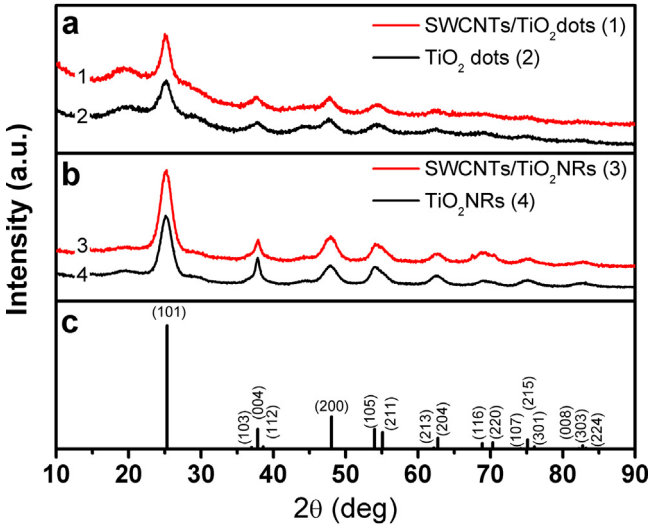

Fig. 2. XRD experimental patterns of (A) SWCNTs/TiO_2 dots (red line 1) and TiO_2 (black line 2); and (B) SWCNRs/TiO_2 NRs (red line 3) and TiO_2 NRs (black line 4). (C) Bragg *hkl* reflections positions for anatase phase.

reveals a definitely different morphology, as, conversely to what observed in the case of SWCNTs/TiO_2 heterostructures, in the case of the mixed sample SWCNT surface stays smooth as in the bare SWCNT sample. In fact distinct areas appear populated by SWCNTs and TiO_2 NRs can be clearly observed. Such experimental evidence unambiguously supports the hypothesis that proposed synthetic approach results in TiO_2 nucleation at the surface of SWCNTs.

XRD experimental profiles of TiO_2 (black lines 2 and 4) and SWCNTs/TiO_2 (red lines 1 and 3) dots and NRs are reported in Fig. 2a and b, respectively. The crystalline nature of the samples was determined by fitting the patterns through a Rietveld-based approach [31] for both dots and NRs crystals of TiO_2 and SWCNTs/TiO_2. The relevant fit curves and parameters are reported in Figure S4 and in Table S1, respectively, in the Supplemenrary Material section. The quantitative Rietveld-based analysis of the diffraction data allowed to ascribe to anatase the crystalline phase nature of the TiO_2 samples.

The broad line-widths were found consistent with the formation of nanosized crystalline domains: of spherical and elongated shape in case of dots and NRs crystals, respectively. Indeed, data collected on the TiO_2 and SWCNTs/TiO_2 NRs, reported in Fig. 2b, clearly showed higher and sharper (0 0 4) reflection with respect of those reported in Fig. 2a. This evidence is consistent with NRs elongated along the [0 0 1] crystallographic direction, and with the TEM results.

Calculation of the refined structure parameters evidenced that the anatase unit cell volume of both TiO_2 and SWCNTs/TiO_2 NRs remains substantially unchanged with respect to the unit cell volume of the corresponding TiO_2 and SWCNTs/TiO_2 dots, as reported in Table S1. The SWCNT presence affects mainly the background of the XRD profiles.

Fig. 3a shows the Raman spectra of SWCNTs/TiO_2 NRs. The SWCNT, which is characterized by radial breathing modes (RBMs) at 148 cm^{-1}, higher frequency modes at 1320 cm^{-1} (D), 1560 cm^{-1} (G^-), 1586 cm^{-1} (G^+), and second-order Raman scattering from D-band variation at 2624 cm^{-1} (G′) [32]. Although the D, G, and G′ modes can be also found in graphite, the RBM is specific to SWCNTs and is representative of the isotropic radial expansion of the tube. The RBM frequency is inversely proportional to the nanotube diameter. The G band is a tangential shear mode of carbon atoms that corresponds to the stretching mode in the graphite plane. The splitting of this mode into G^- and G^+ as a result of the confinement of wave-vectors along the circumference confirms the tube nature of the carbonaceous material but also gives information about its metallic properties. Notably in metallic SWCNTs G^- is characterized by a broad and asymmetric line shape such as that showed in the spectrum. The D band is a longitudinal optical phonon and is known as the disordered or defect mode because a defect is required to elastically scatter in order for the process to conserve momentum. In SWCNTs, this band is activated from the first-order scattering process of sp^2 carbons by the presence of in-plane substitutional hetero-atoms, vacancies, grain boundaries, or other defects, and by finite-size effects. All of these characteristics lower the crystal symmetry of the quasi-infinite lattice.

The vibrational signature of TiO_2 coating of the SWCNT is shown in Fig. 3b. The three strong detected peaks cane be assigned to TiO_2 anatase phase at 400, 515, and 637 cm^{-1} [33,34]. These peaks are rather broaden and the 400 cm^{-1} band is slightly shifted with respect to that of a bulk crystal that is observed at 395 cm^{-1}. The observed line broadening and the concomitant shift were also shown in coupled CdS/TiO_2 systems, and ascribed to the breakdown of the phonon momentum selection rule, specific of the Raman scattering in ordered systems. In the case of very small crystals, this rule is no longer valid as the phonons would be confined in space and all the phonons over the Brillouin zone would contribute to the first order Raman spectra. The weight of the off-centre phonons increases as the crystal size decreases and the phonon dispersion causes an asymmetrical broadening and the shift of the Raman peaks [35].

Representative FT-IR-ATR spectra in the region 4000–600 cm^{-1} of a typical SWCNTs/TiO_2 heterostructure (Fig. 4a) and of SWCNT dispersed in OLEA (Fig. 4b) are reported. Both sample were washed 5 times according to the precipitating procedure described in experimental section to remove uncoordinated OLEA. The spectrum of pure OLEA is also shown for comparison (Fig. 4c). Above 2000 cm^{-1}, the SWCNTs/TiO_2 and SWCNT samples exhibits the antisymmetric and symmetric C–H stretching vibrations (at 2920 and 2850 cm^{-1}, respectively) of the $–CH_2–$ groups in the hydrocarbon chain of OLEA. The shoulder at 2960 cm^{-1} can be associated with the asymmetric stretching of the terminal $–CH_3$ group of the alkyl chain. The weak band at 3008 cm^{-1} attributable to the olefinic C–H stretching visible in pure OLEA is not detectable in SWCNTs/TiO_2 and SWCNT samples probably due to the low amount of OLEA molecule.

Accordingly, the typical O–H broad stretching band centred at 3000 cm^{-1} typical of OLEA dimers visible in pure OLEA sample is

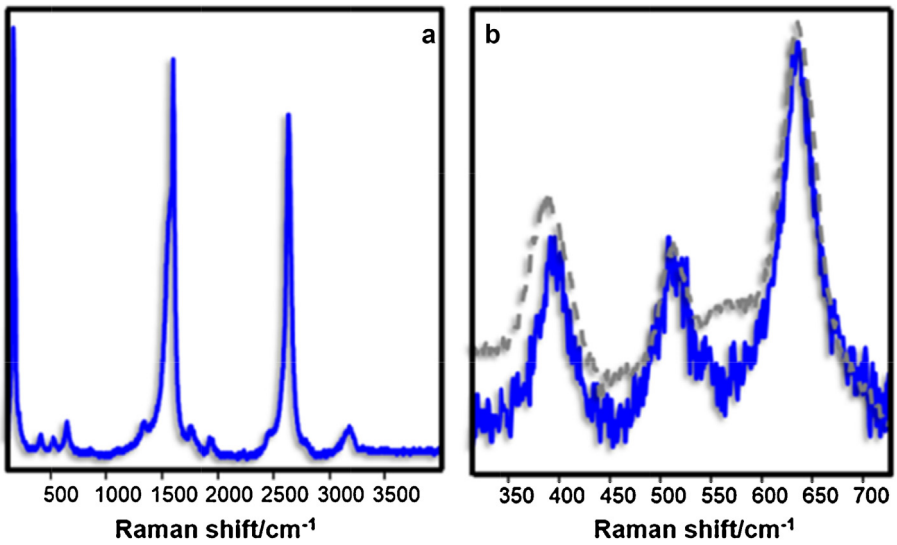

Fig. 3. (A) Raman spectra of the SWCNTs/TiO_2 NRs (633 nm, 10 mW). (B) Raman spectra of free TiO_2 NRs (anatase dotted lines) and SWCNTs/TiO_2 NRs.

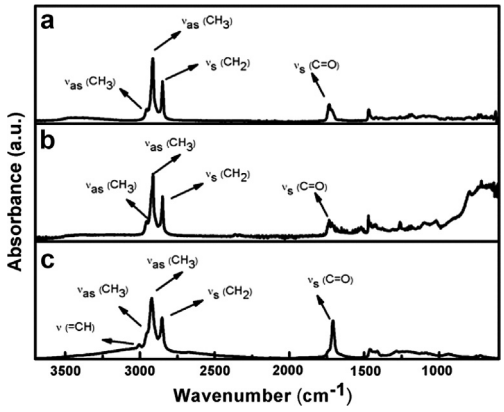

Fig. 4. FT-IR-ATR spectra of SWCNTs (A) and SWCNTs/TiO_2 NRs (B) in the 4000–600 cm^{-1} region after the washing procedure. FT-IR-ATR spectrum of pure OLEA is reported for comparison (C).

not observed in the SWCNTs/TiO_2 and SWCNT samples. The wide absorption below 950 cm^{-1} recorded in the case of SWCNTs/TiO_2 is ascribable to the characteristic vibration of the inorganic Ti–O–Ti network in TiO_2. Interestingly, the weakening of the typical C=O stretching vibration and the absence of O–H stretching at 3300 cm^{-1} in both SWCNTs/TiO_2 and SWCNT samples suggest that the –COOH groups of OLEA are involved in the coordination of surface of both samples [27,36]. Interaction of C=O groups with CNTs has been already reported in literature upon sonication of CNTs in presence of molecules bearing carbonyl groups [36]. We carried out a similar sonication procedure to disperse SWCNTs in OLEA. Therefore residual OLEA molecules result still present on SWCNTs/TiO_2 after repeated washing, thus stabilizing the heterostructure in apolar organic solvents. Besides, such OLEA at TiO_2 surface could play a beneficial role in photocatalysis allowing to further stabilize the photo-induced excited state of TiO_2 nanocrystals, as already demonstrated by a reported EPR study [37].

3.3. SWCNTs/TiO_2 heterostructure growth mechanism

The mechanism behind the growth of TiO_2 NRs and dots was already reported in detail in literature [27]. Rod formation is typically based on anisotropic crystal growth which can occur when surface free energy of the various crystallographic planes differs significantly, thus favouring growth along one specific direction, or, alternatively, when the growth of certain crystallographic planes is somehow prevented [38,39]. In a monosurfactant system, like the investigated reaction mixture, the potential for unidirectional growth of TiO_2 particles could arise from the intrinsic anisotropic reactivity of the titania precursor and from the adsorbing-chelating ligand (i.e. OLEA), which could inhibit the growth along some crystallographic directions. Since titanium alkoxides are known to readily react with carboxylic acids in mild conditions [40], the actual titanium precursor should be titanium oxocarboxyalkoxide which is intrinsically anisotropic [27]. However, such an intrinsic anisotropy, and the consequent control of the shape, can be obtained by tuning the amount of water present in the system. As a matter of fact, a large amount of water directly injected in the flask promoted one-dimensional growth (*fast hydrolysis route*), whereas nearly spherical particles were obtained when water was slowly released from esterification of OLEA and glycerol [27].

In presence of SWCNTs the nucleation and growth of TiO_2 nanocrystals is likely to occur preferentially at the surface of SWCNTs. Indeed, the nucleation of TiO_2 nanocrystals at SWCNT surface is energetically favoured with respect to the formation of novel nuclei in solution in agreement with a well-established principle of the classical nucleation theory stating that the activation energy needed to enlarge pre-existing particles in a solution (i.e. heterogeneous nucleation/growth) is considerably lower than the barrier for the generation of novel nuclei (i.e. homogeneous nucleation) [41]. Thus, it is reasonable that SWCNT suspended in the reaction mixture could act as nucleation seeds for TiO_2 nuclei, promoting heterogeneous growth of NRs or dots at their surface. The formation of distinct TiO_2 nanocrystals on SWCNTs rather than a continuous a TiO_2 shell suggests that, under the investigated conditions, the interfacial energy between SWCNTs and TiO_2 is too high to epitaxial growth of TiO_2 shell. However, provided that enough energy is supplied to the reaction mixture (by thermal heating for instance) the growth of a second material on a pre-existing solid (i.e. SWCNTs) is still favoured. According to this principle several heterodimer structures have been reported in literature [42]. Therefore, in the present case of study, TiO_2 nanocrystals grow in spherical or rod-like shape at SWCNTs surface in order to minimize interfacial strain.

In conclusion, it could be safely proposed that under heating (100 °C) OLEA molecules coordinating SWCNT surface could desorb allowing the titanium oxocarboxyalkoxide already present in the bulk of the reaction mixture to interact with SWCNT surface thus promoting TiO_2 nanocrystal nucleation directly on SWCNT walls. At this stage the reaction proceeds toward the synthesis of dots or NRs following the reaction path already proposed above for bare TiO_2 nanocrystals. Due to the large amount of OLEA coordinated TiO_2 nanocrystals grown on SWCNT surfaces, the as-prepared SWCNTs/TiO_2 show a dispersibility in organic solvents similar to that of TiO_2 nanocrystals. Concomitantly, the micrometric size of the SWCNTs (5 μm) allows to easy recovery the heterostructures by centrifugation without adding any precipitating agents.

3.4. Characterization of photoactivity under UV irradiation

The photoactivity of SWCNTs/TiO_2 NRs and dots has been tested by means of a standard oxidative reaction, involving the discolouration of the azo-dye methyl red (MR) dispersed in water, under UV irradiation and ambient conditions, already widely investigated in literature [15,43,44]. Experiments under visible light were also performed to investigate the capability of SWCNTs to improve the visible light activity of TiO_2. Experiments in the dark were also carried out to assess the effect of dye absorption on the discolouration rate demonstrating a negligible contribution to the overall discolouration observed (Figure S5 and in Supplementary Material).

Fig. 5 reports the kinetic of MR discolouration, under UV irradiation, as $\ln(C_0/C)$ vs reaction time. The plot gives rise to a straight line whose slope k is the apparent rate constant. Experimental results clearly highlight that the reaction course is much faster in presence of SWCNTs/TiO_2 based catalysts than in presence of bare TiO_2 NRs, dots, TiO_2 P25 or SWCNTs, respectively. In addition, the kinetic constants point out a 1.7 time increase of the reaction rate of SWCNTs/TiO_2 dots with respect to TiO_2 dots and a 10-fold increase with respect to SWCNTs.

SWCNTs/TiO_2 NRs show a reaction rate 1.34 times higher than bare NRs and 7 times higher than SWCNTs. Moreover, the photoactivity of SWCNTs/TiO_2 heterostructures compared to a broadly accepted standard TiO_2 catalyst (TiO_2 P25) results in a two-fold increase in reaction rate for SWCNTs/TiO_2 NRs and three-fold increase for SWCNTs/TiO_2 dots. The logarithmic plot of the mixture of SWCNTs and pre-synthesized TiO_2 dots or TiO_2 NRs overlaps the one obtained for the reaction assisted by the bare TiO_2 NCs. The kinetic constant of TiO_2 dots is $0.052 \pm 0.003\ min^{-1}$, while the respective mixture reported a kinetic constant of $0.051 \pm 0.001\ min^{-1}$, whereas TiO_2 NRs and the mixture TiO_2 NRs and SWCNTs have shown a kinetic constant of $0.044 \pm 0.002\ min^{-1}$ and $0.047 \pm 0.001\ min^{-1}$, respectively (Table 1). Therefore a simple

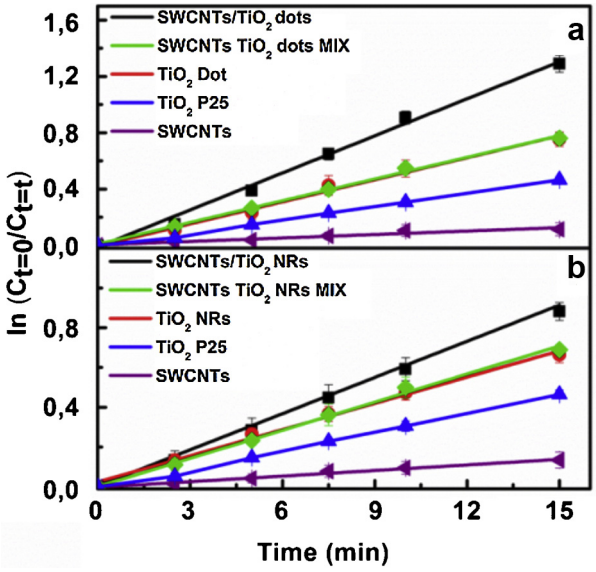

Fig. 5. Comparison of MR discolouration rates in presence SWCNTs/TiO_2 dots; SWCNTs/TiO_2 NRs, TiO_2 dots, TiO_2 NRs, CNTs and TiO_2 P25. Experiments were carried out at pH 6.5 under UV irradiation. MR concentration has been evaluated by monitoring the absorbance intensity at 430 nm (pH 6.2). Experimental data are reported as mean values of 5 replicates ± standard deviation.

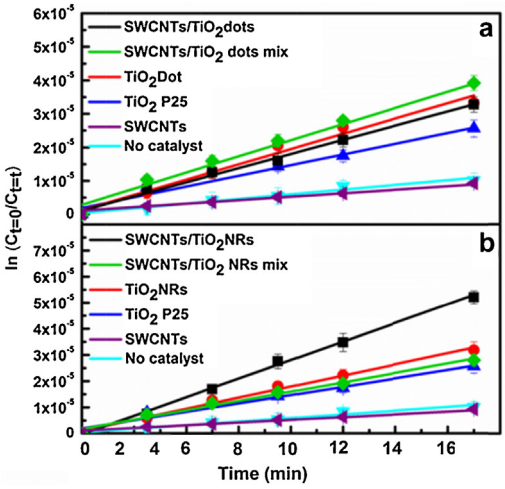

Fig. 6. MR discolouration rates in presence SWCNTs/TiO_2 dots; SWCNTs/TiO_2 NRs, TiO_2 dots, TiO_2 NRs, CNTs, TiO_2 P25, bare SWCNRs and mixture of pre-synthesized TiO_2 nanocrystals and SWCNTs. Experiments have been carried out at pH 6.5 under visible light irradiation. MR concentration has been evaluated by monitoring the absorbance intensity at 430 nm (pH 6.5). Experimental data are reported as mean values of 5 replicates ± standard deviation.

mixing of pre-synthesized TiO_2 nanocrystals and SWCNT does not provide a significant enhancement of the photocatalytic performances for either dots or NRs. No reliable comparison can be done between SWCNTs/TiO_2 NRs and dots due to the different amount of Ti precursor used in the synthesis which results in different shape of nanoparticles. Therefore an equal number of TiO_2 moles is not equivalent to the amount of TiO_2 nanocrystals samples, which present two distinct morphologies.

The whole set of results obtained under UV irradiation highlights the synergistic effect of TiO_2 and SWCNTs which can be explained by considering different factors. SWCNTs show a metallic behaviour as demonstrated by Raman data. It has been reported that noble metals in contact with semiconductor particles could improve the photocatalytic electron transfer processes at the semiconductor interface [45].

At the interface of the two materials, electrons flow from one material to the other (from the Fermi level with higher value to that with lower value) to align the Fermi energy levels. In the case of a metal, having a higher work function than the n-type semiconductor, such as TiO_2, electrons flow from the semiconductor into the metal to adjust the Fermi energy levels.

This results in the formation of a Schottky barrier, with an excess of negative charge on the metal and an excess positive charge on the semiconductor. In between, at the interface of the two components, a depletion layer maintains charge separation [45]. Indeed electrons could accumulate in a large extent within the SWCNTs thus improving the efficiency of electron–hole separation and preventing recombination [46,47]. It has been demonstrated for Ag or Au nanoparticles which strongly improve the photoactivity of TiO_2 NRs [15,17,48,49]. Due to the metallic behaviour of SWCNTs a similar mechanism could be reasonably proposed also for our SWCNTs/TiO_2 heterostructures [7,19,50].

3.5. Characterization of photoactivity under visible light irradiation

SWCNTs could also act as sensitizer, enhancing the absorption of visible light [7,51]. Therefore the MR discolouration has been investigated also upon irradiation with visible light. A first survey of the logarithmic plots, in Fig. 6, shows that both SWCNTs/TiO_2 dots and SWCNTs/TiO_2 NRs exhibit photocatalytic activity under visible light.

In particular, a significative improvement was observed in the photocatalytic activity of SWCNTs/TiO_2 NRs heterostructures compared to bare TiO_2 NRs being the kinetic constants $0.035 \pm 0.001\ min^{-1}$ and $0.021 \pm 0.001\ min^{-1}$, respectively (Table 2). The simple mix of SWCNTs and TiO_2NRs shows again a photocatalytic activity close to bare TiO_2NRs, with a kinetic constant $0.018 \pm 0.001\ min^{-1}$. A different trend has been observed for the photocatalytic behaviour of SWCNTs/TiO_2 dots heterostructure under visible light. The kinetic constants SWCNTs/TiO_2 dots, bare TiO_2 dots and the mix of SWCNTs and TiO_2 dots are quite close to each other ($0.020 \pm 0.001\ min^{-1}$ $0.023 \pm 0.001\ min^{-1}$ and $0.024 \pm 0.001\ min^{-1}$, respectively) thus showing a comparable photocatalytic behaviour, irrespective of the presence of SWCNTs.

Table 1
Kinetic constants of MR discolouration under UV light.

Catalyst	$k\ (min^{-1})$
SWCNTs/TiO_2 dots	0.088 ± 0.004
TiO_2 dots	0.052 ± 0.003
SWCNTs/TiO_2 NRs	0.059 ± 0.001
TiO_2 NRs	0.044 ± 0.002
TiO_2 P25	0.032 ± 0.002
SWCNT	0.008 ± 0.003
SWCNTs TiO_2 dots mix	0.051 ± 0.001
SWCNTs TiO_2 NRs mix	0.047 ± 0.002

Table 2
Kinetic constants of MR discolouration under visible light.

Catalyst	$k\ (min^{-1})$
SWCNTs/TiO_2 dots	0.021 ± 0.001
TiO_2 dots	0.023 ± 0.001
SWCNTs/TiO_2 NRs	0.035 ± 0.001
TiO_2 NRs	0.021 ± 0.001
TiO_2 P25	0.016 ± 0.001
SWCNT	0.006 ± 0.001
SWCNTs/TiO_2 dots MIX	0.025 ± 0.002
SWCNTs/TiO_2 NRs MIX	0.018 ± 0.002

The mechanism behind the visible light activity of TiO_2-CNTs heterostructures is still under debate and controversial hypotheses have been proposed [7,19]. The most popular hypothesis deal with (i) a sensitization mechanism [52] similar to that proposed for coupled semiconductor, and with (ii) doping-like mechanism [7]. According to sensitization mechanism, electrons can be photogenerated in CNTs and then injected into the conduction band of the TiO_2, allowing for the formation of superoxide radicals by adsorbed molecular oxygen finally leading to hydroxyl radicals [53]. Once this occurs, the positively charged CNTs remove an electron from the valence band of the TiO_2 leaving a hole. The now positively charged TiO_2 can then reacts with adsorbed water to form hydroxyl radicals. The doping-like mechanism takes into account two distinct contributions from the TiO_2-CNT heterostructures. One is the carbon–oxygen–titanium bond occurring at CNT-TiO_2 interface in which C acts as a dopant extending the light absorption of TiO_2 to longer wavelengths. Therefore, such a sort of C impurity could potentially lead to the improvement of the photocatalytic activity in the visible range, similarly to carbon-doped titania. The second contribution is the electronic configuration of the CNTs. Indeed, it has been demonstrated that CNTs with high electrical conductivity and few defects provide much stronger enhancement of the photocatalytic activity than CNTs with high amount of defect and low conductivity [7]. SWCNTs used in the present work demonstrated a metallic behaviour (according to Raman spectra), thus high electrical conductivity and efficient charge transfer can be reasonably expected according to the sensitization mechanism [54]. However, taking into account that SWCNTs/TiO_2 dots do not show an increase of photocatalytic activity under visible irradiation despite they demonstrated very good performances under UV irradiation, and considering that on the contrary SWCNTs/TiO_2 NRs show enhancement of photoactivity both under UV and visible irradiation a doping like mechanism could be also invoked. Indeed, the doping like mechanism invokes the presence of defect states in TiO_2 gap due to the carbon–oxygen–titanium bond at the SWCNT/TiO_2 interface. Such defect states could be useful for visible light activated photocatalysis but should be detrimental for UV activated processes because they could act as trap states [55]. In addition, the probability of occurrence of such defect states should increase with the increasing of contact surface area between SWCNT and TiO_2. In our system, TiO_2 NRs due to their elongated shape can reasonably provide a larger surface for contact with SWCNTs and hence a much dense packing, finally allowing efficient charge transfer.

On the contrary, due to geometrical considerations, the contact area between spherical like TiO_2 nanocrystals and SWCNTs is much lower therefore a lower level of "doping" is expected.

As a result, SWCNTs/TiO_2 dots show strong enhancement of photoactivity under UV irradiation where the process is only driven by e^-/h^+ separation, whereas SWCNTs/TiO_2 NRs which could take advantage from both e^-/h^+ separation and doping show enhanced performances under both UV and visible light irradiation. Taking into account the above reported considerations, under visible light irradiation the bottle neck of the process should be the amount of defect states in TiO_2 band gap yielded by C—O—Ti bonds. In fact, several authors reported that a close contact between TiO_2 and CNTs is the *sine qua non conditio* for effective improving photocatalytic performances [22,23].

4. Conclusion

In summary, a colloidal synthetic route for the *in situ* growth of anisotropic (nanorods) and isotropic (dots) anatase TiO_2 nanocrystals onto the surface of SWCNTs has been proposed, allowing the fine tuning of the nanocrystal geometry just in one step, without any post-synthesis thermal treatment. Remarkably, the obtained heterostructures are dispersible in organic solvents, providing a promptly processable material, which can be easily recovered by centrifugation, without adding any precipitating agent. The SWCNTs/TiO_2 heterostructure shows an enhanced photocatalytic activity with respect to bare TiO_2, either dots and NRs, SWCNTs and TiO_2 P25, used in this work as reference material. The significant photocatalytic activity has been explained in terms of interfacial charge transfer between TiO_2 and SWCNTs, being able, at same time, to prevent electron–hole recombination and to induce sensitization phenomena. Under visible light, the investigated SWCNTs/TiO_2 heterostructure presented a photocatalytic activity higher than the TiO_2 P25, in particular the SWCNTs/TiO_2 NRs exhibits a kinetic constant, 1.6 times faster than bare TiO_2 NRs and 2 times higher than TiO_2 P25, thus confirming the synergistic effect between SWCNTs and TiO_2 NRs arising from the close contact between the surfaces of the two components.

The proposed SWCNTs/TiO_2 heterostructures demonstrate very promising candidates for photocatalysis and other energy conversion-related applications, including water splitting and photovoltaics.

Acknowledgements

The authors thank B. Rodríguez-González for their help on the HRTEM characterization. This work was partially funded by the EC-funded 7th FP projects LIMPID (Grant n. 310177) and ORION (CP-IP 229036-2), by Apulia Region funded Project RELA-VALBIOR, Network of Laboratories for Scientific Research (Italy), by the Spanish Ministerio de Economía y Competitividad (CTQ2011-23167), and the FIRB 2009/2010 project "Rete integrata per la Nano Medicina (RINAME)"–RBAP114AMK_006. Rocco Lassandro and Giovanni Filograsso are acknowledged for technical and administrative support with the Bruker D8 Discover diffractometer.

Appendix A. Supplementary data

Supplementary data associated with this article can be found, in the online version, at http://dx.doi.org/10.1016/j.apcatb.2014.10.030.

References

[1] H. Tong, S. Ouyang, Y. Bi, N. Umezawa, M. Oshikiri, J. Ye, Adv. Mater. 24 (2012) 229–251.
[2] Y. Paz, Appl. Catal. B 99 (2010) 448–460.
[3] J. Kiwi, C. Pulgarin, Catal. Today 151 (2010) 2–7.
[4] M. Grätzel, Acc. Chem. Res. 42 (2009) 1788–1798.
[5] X. Chen, S. Shen, L. Guo, S.S. Mao, Chem. Rev. 110 (2010) 6503–6570.
[6] X. Chen, S.S. Mao, Chem. Rev. 107 (2007) 2891–2959.
[7] K. Woan, G. Pyrgiotakis, W. Sigmund, Adv. Mater. 21 (2009) 2233–2239.
[8] A. Fujishima, X. Zhang, D.A. Tryk, Surf. Sci. Rep. 63 (2008) 515–582.
[9] A.L. Linsebigler, G. Lu, J.T. Yates, Chem. Rev. 95 (1995) 735–758.
[10] H.G. Yang, C.H. Sun, S.Z. Qiao, J. Zou, G. Liu, S.C. Smith, H.M. Cheng, G.Q. Lu, Nature 453 (2008) 638–641.
[11] X. Han, Q. Kuang, M. Jin, Z. Xie, L. Zheng, J. Am. Chem. Soc. 131 (2009) 3152–3153.
[12] U. Diebold, Surf. Sci. Rep. 48 (2003) 53–229.
[13] M. Pelaez, N.T. Nolan, S.C. Pillai, M.K. Seery, P. Falaras, A.G. Kontos, P.S.M. Dunlop, J.W.J. Hamilton, J.A. Byrne, K. O'Shea, M.H. Entezari, D.D. Dionysiou, Appl. Catal. B 125 (2012) 331–349.
[14] W. Guo, F. Zhang, C. Lin, Z.L. Wang, Adv. Mater. 24 (2012) 4761–4764.
[15] F. Petronella, E. Fanizza, G. Mascolo, V. Locaputo, L. Bertinetti, G. Martra, S. Coluccia, A. Agostiano, M.L. Curri, R. Comparelli, J. Phys. Chem. C 115 (2011) 12033–12040.
[16] F.Z. Huang, M.F. Zhou, Y.B. Cheng, R.A. Caruso, Chem. Mater. 18 (2006) 5835–5839.
[17] Z. Bian, T. Tachikawa, P. Zhang, M. Fujitsuka, T. Majima, J. Am. Chem. Soc. 136 (2014) 458–465.
[18] M. Cargnello, M. Grzelczak, B. Rodrıǵuez-González, Z. Syrgiannis, K. Bakhmutsky, V. La Parola, L.M. Liz-Marzán, R.J. Gorte, M. Prato, P. Fornasiero, J. Am. Chem. Soc. 134 (2012) 11760–11766.
[19] R. Leary, A. Westwood, Carbon 49 (2011) 741–772.
[20] J. Yu, T. Ma, S. Liu, Phys. Chem. Chem. Phys. 13 (2011) 3491–3501.

[21] Z. Li, B. Gao, G.Z. Chen, R. Mokaya, S. Sotiropoulos, G. Li Puma, Appl. Catal. B 110 (2011) 50–57.
[22] Y. Yao, G. Li, S. Ciston, R.M. Lueptow, K.A. Gray, Environ. Sci. Technol. 42 (2008) 4952–4957.
[23] B. Gao, G.Z. Chen, G. Li Puma, Appl. Catal. B 89 (2009) 503–509.
[24] W. Guo, C. Xu, X. Wang, S. Wang, C. Pan, C. Lin, Z.L. Wang, J. Am. Chem. Soc. 134 (2012) 4437–4441.
[25] M.A. Correa-Duarte, J. Pérez-Juste, A. Sánchez-Iglesias, M. Giersig, L.M. Liz-Marzán, Angew. Chem. Int. Ed. 44 (2005) 4375–4378.
[26] M. Sanles-Sobrido, M.A. Correa-Duarte, S. Carregal-Romero, B. Rodríguez-González, R.n.A. Álvarez-Puebla, P. Hervés, L.M. Liz-Marzán, Chem. Mater. 21 (2009) 1531–1535.
[27] P.D. Cozzoli, A. Kornowski, H. Weller, J. Am. Chem. Soc. 125 (2003) 14539–14548.
[28] G.J. Thomas, D.A. Agard, Biophys. J. 46 (1984) 763–768.
[29] F. Milano, L. Gerencsér, A. Agostiano, L. Nagy, M. Trotta, P. Maróti, J. Phys. Chem. B 111 (2007) 4261–4270.
[30] X. Peng, J. Chen, J.A. Misewich, S.S. Wong, Chem. Soc. Rev. 38 (2009) 1076–1098.
[31] Refinement of powder and single-crystal diffraction data.
[32] M.S. Dresselhaus, G. Dresselhaus, R. Saito, A. Jorio, Phys. Rep. 409 (2005) 47–99.
[33] M.B. Yahia, F. Lemoigno, T. Beuvier, J.-S. Filhol, M. Richard-Plouet, L. Brohan, M.-L. Doublet, J. Chem. Phys. 130 (2009) 204501–204511.
[34] J.C. Tristão, F. Magalhães, P. Corio, M.T.C. Sansiviero, J. Photochem. Photobiol. A-Chem. 181 (2006) 152–157.
[35] D. Bersani, P.P. Lottici, X.-Z. Ding, Appl. Phys. Lett. 72 (1998) 73–75.
[36] Y.-J. Baek, Q. Hu, Y.-S. Lim, C.J. Kang, H.H. Lee, T.-S. Yoon, Phys. Stat. Solidi A 210 (2013) 2622–2627.
[37] M. Fittipaldi, M.L. Curri, R. Comparelli, M. Striccoli, A. Agostiano, N. Grassi, C. Sangregorio, D. Gatteschi, J. Phys. Chem. C 113 (2009) 6221–6226.
[38] T. Placido, R. Comparelli, F. Giannici, P.D. Cozzoli, G. Capitani, M. Striccoli, A. Agostiano, M.L. Curri, Chem. Mater. 21 (2009) 4192–4202.
[39] F. Giannici, T. Placido, M.L. Curri, M. Striccoli, A. Agostiano, R. Comparelli, Dalton Trans. (2009) 10367–10374.
[40] T.J. Boyle, R.P. Tyner, T.M. Alam, B.L. Scott, J.W. Ziller, B.G. Potter, J. Am. Chem. Soc. 121 (1999) 12104–12112.
[41] M. Casavola, R. Buonsanti, G. Caputo, P.D. Cozzoli, Eur. J. Inorg. Chem. 2008 (2008) 837–854.
[42] P.D. Cozzoli, T. Pellegrino, L. Manna, Chem. Soc. Rev. 35 (2006) 1195–1208.
[43] R. Comparelli, E. Fanizza, M.L. Curri, P.D. Cozzoli, G. Mascolo, R. Passino, A. Agostiano, Appl. Catal. B-Environ. 55 (2005) 81–91.
[44] R. Comparelli, P.D. Cozzoli, M.L. Curri, A. Agostiano, G. Mascolo, G. Lovecchio, Water Sci. Technol. 49 (2004) 183–188.
[45] V. Subramanian, E. Wolf, P.V. Kamat, J. Phys. Chem. B 105 (2001) 11439–11446.
[46] P.D. Cozzoli, R. Comparelli, E. Fanizza, M.L. Curri, A. Agostiano, D. Laub, J. Am. Chem. Soc. 126 (2004) 3868–3879.
[47] P.D. Cozzoli, M.L. Curri, A. Agostiano, Chem. Commun. (2005) 3186–3188.
[48] P.D. Cozzoli, E. Fanizza, R. Comparelli, M.L. Curri, A. Agostiano, D. Laub, J. Phys. Chem. B 108 (2004) 9623–9630.
[49] A.A. Ismail, D.W. Bahnemann, I. Bannat, M. Wark, J. Phys. Chem. C 113 (2009) 7429–7435.
[50] A. Kongkanand, P.V. Kamat, ACS Nano 1 (2007) 13–21.
[51] G. An, W. Ma, Z. Sun, Z. Liu, B. Han, S. Miao, Z. Miao, K. Ding, Carbon 45 (2007) 1795–1801.
[52] W. Wang, P. Serp, P. Kalck, J.L. Faria, J. Mol. Catal. A-Chem. 235 (2005) 194–199.
[53] M.R. Hoffmann, S.T. Martin, W. Choi, D.W. Bahnemann, Chem. Rev. 95 (1995) 69–96.
[54] R. Long, J. Phys. Chem. Lett. 4 (2013) 1340–1346.
[55] M.Y. Guo, F. Liu, Y.H. Leung, A.M.C. Ng, A.B. Djurišić, W.K. Chan, Curr. Appl. Phys. 13 (2013) 1280–1287.